Biomass waste-based material: Electrochemical performance and CO_2 uptake capability

Kieu Trang Trinh

kieutrangtrinh.edu@gmail.com

Kyushu Institute of Technology: Kyushu Kogyo Daigaku https://orcid.org/0000-0002-0588-5165

Dimitrios Kalderis

Hellenic Mediterranean University: Elleniko Mesogeiako Panepistemio

Toshiki Tsubota

Kyushu Institute of Technology: Kyushu Kogyo Daigaku

Research Article

Keywords: biochar, activated carbon, CO2 adsorptions, electric double layer capacitor, supercapacitor, air pollution, shortage of energy storage devices

Posted Date: March 18th, 2024

DOI: https://doi.org/10.21203/rs.3.rs-3935417/v1

Abstract

This study investigates the utilization of Japanese cedar bark (JCB) waste for the preparation of chemically-activated porous biochar materials using K_2CO_3 (xKC, where x represents the K_2CO_3 to JCB weight ratio). The research explores the versatile applications of these biochar materials, specifically focusing on CO_2 adsorption and as supercapacitors. A thorough analysis employing chemical composition, microstructure, gas adsorption isotherms is conducted to gain insights into the surface and structural properties of the materials. The CO_2 adsorption and electrochemical performance are assessed through isotherms at 298K and various electrochemical techniques. The study identifies functional groups and pore structures as critical factors influencing the adsorption capacity of xKC. Among the samples, 2KC demonstrated the optimal CO_2 adsorption (approximately 180 mg g^{-1}), while 6KC exhibited superior electrochemical stability, with a maximum capacitance of around 210 F g^{-1} at 10 mA g^{-1}. This comprehensive exploration provides valuable insights into the impact of material properties on both CO_2 adsorption and electrochemical behavior in K_2CO_3-activated biochar from JCB, suggesting promising interdisciplinary applications.

1. Introduction

In the face of escalating environmental challenges, ranging from climate change and global warming to pervasive air pollution, the imperative to address these issues has become a global priority (Zhou et al. 2024). A collective effort from all sectors of society is essential to mitigate the root causes of ecological problems. Amidst this backdrop, the quest for effective CO_2 adsorption methods has been a longstanding focus within environmental research (Khoshraftar et al. 2023). Concurrently, there has been substantial exploration in the power industry to enhance the efficiency of energy storage devices, encompassing batteries, capacitors, and supercapacitors, all crafted from environmentally sustainable materials (Teoh et al. 2023). Within the realm of materials science, the utilization of agricultural and industrial biomass wastes to create porous biochar materials has emerged as a promising pathway for practical applications (Trinh and Tsubota 2023). Notably, cedar bark, recognized for its high lignin and cellulose content (Umemura et al., 2014), stands out as a potential precursor for porous carbon materials, drawing significant attention in research circles. The activation process using eco-agent K_2CO_3, a well-established activator, has been extensively employed in creating porous activated materials. Previous research has explored K_2CO_3-activated carbon derived from bamboo (Khuong et al. 2022), coconut shell (Yue et al. 2018) and coffee ground (Kim et al. 2020) for CO_2 adsorption, as well as other materials like willow bark (Hobisch et al. 2020), tree bark (Momodu et al. 2017), and cedar bark (Trinh and Tsubota 2023) for supercapacitor applications. However, a noteworthy gap exists in the literature concerning K_2CO_3-activated biochar derived from cedar bark, particularly in its dual application for both CO_2 adsorption and as an electrode material for Electric Double Layer Capacitors (EDLC). This study aims to bridge this gap by proposing the fabrication of porous biochar materials from Japanese Cedar bark, an abundant biomass waste, activated by K_2CO_3 - an environmentally friendly activator. K_2CO_3 is renowned for its

environmentally friendly attributes, attributed to its common usage in the food industry (Yue et al. 2023). The primary objective is to assess the material properties related to CO_2 adsorption capability and electrochemical performance for supercapacitor electrodes, shedding light on the untapped potential of this novel biomaterial in addressing contemporary environmental and energy storage challenges.

2. Experimental part

The experimental procedures commenced with the acquisition of Japanese Cedar bark (JCB) from Imari Wood Market Co., Ltd (Kyushu, Japan). Subsequently, the JCB was washed with distilled water, dried at 105°C for 48 hours, and subsequently ground into a finely powdered form by a grain grinder. A 1 g portion of pretreated JCB powder was then thoroughly mixed in a water solution containing a variable amount (x g) of the environmentally friendly activator K_2CO_3 (where x ranged from 0 to 6). This mixture was stirred and allowed to homogenize for 8 hours before undergoing a drying process at 105°C for 2 days. Following the preparation phase, the dried sample underwent activation at 800°C in a tubular electric furnace, in a N_2 atmosphere at a flow rate of 0.5 L min^{-1}. The selection of the activation temperature was based on JCB's thermal behavior, as determined in previous studies (Trinh and Tsubota 2023). Post-activation, the samples were washed thoroughly with hot distilled water to eliminate excess activators (residual potassium). Subsequently, the washed samples were dried at 105°C for an additional 24 hours. The former was denoted as "xKC," where "KC" represented K_2CO_3, and "x" indicated the activation ratio (x g of K_2CO_3 per 1 g of JCB, with values ranging from 0 to 6). Non-activated biochar was named as 0KC and K_2CO_3-activated samples as xKC, with value of x lager than 0 named as A-xKC.

Characterization of all samples involved microstructural analyses through Raman spectroscopy (NRS-5100, JASCO Corporation, Japan), and scanning electron microscopy (SEM) (Japan Electronics Co., Ltd JSM-6701F). The surface elemental composition was determined using X-ray Photoelectron Spectroscopy (XPS) (Kratos AXIS Nova, Shimadzu, Japan). Gas adsorption behavior was evaluated through N_2 adsorption isotherms at 77 K using a BELSORP analysis program (BELSORP mini II, MicrotracBEL, Japan). Porosity properties were assessed through the BET (Brunauer-Emmet-Teller) method, micropore (MP) plots, and Barrett-Joyner-Halenda (BJH) plots. Additionally, CO_2 adsorption isotherms at 298 K were measured to estimate the CO_2 adsorption capacity. To comprehend the CO_2 adsorption mechanism, Langmuir and Freundlich models were applied. Electrochemical performance evaluation involved cyclic voltammetry (CV) and galvanostatic charge-discharge (GCD) processes in three-electrode cells, utilizing Pt plate, Ag/AgCl, and 1 M H_2SO_4 solution as a counter electrode, a reference electrode, and an electrolyte, respectively. Furthermore, a Ragone plot of 6KC was constructed based on its GCD data to assess the practical application for an Electric Double Layer Capacitor (EDLC) electrode. All calculations pertaining to electrochemical performance assessments were based on formulas referenced from previous research (Trinh and Tsubota 2023).

3. Results and discussion

3.1 Material characteristics

Figure 1a presents the Raman spectra of the activated biochar samples, showcasing two characteristic peaks at 1350 cm^{-1} and 1590 cm^{-1}, corresponding to the D-band and G-band, respectively. The sp^2 C vibration in the graphite interlayer and the vibration of C with a dangling bond in the plane of the disordered graphite ring structure were denoted by the D- and G-bands, respectively (Yang et al. 2018). The ratio of the peak areas of the D-band to the G-band (*Ls*) is commonly used to assess the degree of disorder in carbon materials, the lower A_D/A_G ratio indicates an increase in the higher degree of order in carbon structures (Trinh and Tsubota 2023). The A_D/A_G ratio increased significantly by 19–24% in A-xKC samples compared to 0KC, reaching a maximum at 2KC of 4.07 before decreasing to 3.88 in 6KC, indicating that as the content of K_2CO_3 increased, so did the percentage of ordered carbon. The presence of aromatic carbon structures which may increase the van der Waals forces between the biochar matrix and adsorbent and hence increase the physisorption (Yang et al. 2018), so 6KC could have better physisorption than 2KC. The XPS spectra (Fig. 1b) revealed characteristic peaks for biochar materials, specifically C1s and O1s. The absence of any discernible peaks related to potassium (K) confirms the efficacy of the post-activation cleaning process in eliminating all residual activator from the sample surface. The O/C ratio, calculated based on the atomic percentage of oxygen to carbon, increased by 160–200% with the addition of K_2CO_3, indicating that the activation process resulted in oxygen-containing functional groups on the surface of A-xKC such as carboxyl, phenol, carbonyl and quinone. These functional groups enhance CO_2 chemisorption due to stronger electrostatic attraction or hydrogen bonding interaction with CO_2 (Igalavithana et al. 2020). Oxygen-containing functional groups also enhance the wettability of electrodes in aqueous electrolytes (Chen et al. 2020). The maximum O/C ratio of 0.15 was observed in 2KC, decreasing to 0.13 in 4KC and 6KC, so 2KC was expected to have the optimum performance in both CO_2 adsorption and electrochemical application.

The N_2 adsorption isotherms at 77 K in Fig. 2a, demonstrate a significant increase in N_2 volume with added K_2CO_3, ranging from *ca.* 100 cm^3 (STP) g^{-1} (0KC) to maximum *ca.* 600 cm^3 (STP) g^{-1} (2KC), indicating that the activator could help improve the specific surface areas and the adsorption ability of A-xKC. Special sections of the N_2 adsorption isotherms of each sample such as steep increases at low relative pressure $p/p_0 < 0.03$, hysteresis loops at medium relative pressure, and vertical rises at high relative pressure $p/p_0 > 0.95$ allow predictions regarding the presence and changing of micropores, mesopores, and macropores, respectively (Trinh and Tsubota 2023). The changing shapes and size of these special sections in Fig. 2a, indicate that the addition of K_2CO_3 increased the amount of micropores, mesopores and macropores on the surface of A-xkC sample compared to 0KC, and when the activator content changed, only the quantity of mesopore and macropore changed, whereas the quantity of micropores remained practically unchanged. Figure 2a shows that 2KC is expected to have the most micropores, mesopores and macropores. The influence of pore structures on the surface of each sample will be discussed in detail later. Figure 2b displays the calculated S_{BET} and pore volumes based on N_2 adsorption isotherms at 77 K. S_{BET} and V_{pore} of A-xKC increased significantly compared to 0KC that could

be the result of chemical reaction between K_2CO_3 with C in the raw material (Heidarinejad et al. 2020). The S_{BET} and V_{micro} values in xKC slightly increased with the K_2CO_3 content, achieving the maximum values of of 1600 $m^2\ g^{-1}$ and *ca.* 0.63 $cm^3\ g^{-1}$, at 6KC respectively, while the optimum V_{total} and V_{meso} values were achieved at 2KC, *ca.* 0.93 and *ca.* 0.41 $cm^3\ g^{-1}$, respectively. This opposite trendcould be explained by the collapse of small mesopores and the generation of larger mesopores or even macropores (Trinh and Tsubota 2023). The S_{BET} and V_{pore} values in this research were higher than several previous K_2CO_3-activated materials derived from coconut shell (Yue et al. 2018) and coffee grounds (Kim et al. 2020).

In Fig. 3, a comprehensive investigation of pore size distributions is presented, utilizing N_2 adsorption isotherms at 77 K along with Micropore (MP) and Barrett-Joyner-Halenda (BJH) plots, complemented by SEM images. The figure provides a visual representation of the surface characteristics from micro to macro scale. Notably, the distinctive surface pore structure of A-xKC is prominently displayed, encompassing micro, meso, and macropores. In contrast, 0KC predominantly exhibits micropores, underscoring the significant impact of the activation process on the diversity of surface pores. The hierarchical pore structure observed in A-xKC, extending from micro to macro scales, is anticipated to positively influence the adsorption capacity of these materials, aligning with previous studies (Trinh and Tsubota 2023). In addition, subtle differences in pore sizes between the A-xKC samples could result in significant variations in their adsorption performance (Khuong et al. 2022). Examining the BJH plots in Fig. 3, it is evident that the mesopore sizes of A-xKC samples primarily fall within the 2–4 nm range. Particularly noteworthy is the observation that sample 2KC exhibited a larger mesopore volume compared to the other samples and also included mesopores with diameters exceeding 10 nm. The presence of such large mesopores, although not dominant in quantity, can be attributed to the collapse process of the mesopores within the 2–4 nm range. This finding is consistent with previous research (Trinh and Tsubota 2023). As the K_2CO_3 content increased, the breakdown rate of these mesopores accelerated, leading to a rapid decrease in mesopore volume. This phenomenon was particularly evident in samples 4KC and 6KC, where the reduction in V_{meso} was accompanied by an increase in the presence of macropores as observed in SEM images. These intricate variations in the pore structure further contribute to the understanding of the adsorption dynamics and electrochemical performance variations observed across different activation ratios, shedding light on the interplay between activation conditions and resulting material characteristics.

3.2 CO_2 adsorption performance

To gain deeper insights into the CO_2 adsorption mechanism and surface pore structure of the activated biochar samples, the CO_2 isotherm adsorption data were fitted in two well-established models: Langmuir and Freundlich. The Langmuir model, recognized as a monolayer adsorption model, and the Freundlich model, known for multilayer adsorption (Igalavithana et al. 2020). Table 1 indicates that the A-xKC exhibited a higher R^2 value for the Freundlich model, whereas 0KC had a higher R^2 for the Langmuir

model. This distinction validates that the CO_2 adsorption mechanism in xKC samples is characterized by multilayer adsorption, while 0KC predominantly features monolayer adsorption. This observation aligns with the diverse and more extensive pore structure on the A-xKC surface, as detailed in Fig. 3. Figure 4b provides a simulation illustrating the correlation between the change in CO_2 adsorption capacity and the alterations in the pore structure of the sample surface after K_2CO_3 addition. Figure 4a showcases a significant increase in CO_2 adsorption volume at 298 K in A-xKC samples, peaking at approximately 180 mg g^{-1} in 2KC. Both the A_D/A_G and O/C ratios derived from Raman and XPS data in Fig. 1b reached their maximum values at 2KC, affirming the superior CO_2 chemisorption capacity of this sample. The achieved capacity of 180 mg g^{-1} of 2KC is relatively similar to values obtained by other K_2CO_3 activated biochar, derived from bamboo (Khuong et al. 2022), coconut shell (Yue et al. 2018) and coffee ground (Kim et al. 2020), confirming the effectiveness of K_2CO_3 activation on CO_2 adsorption ability. Figure 5a substantiates the earlier hypothesis that the amount of CO_2 adsorbed correlates with the changes in micropore and mesopore volumes. As micro and mesopore volumes increased, the amount of CO_2 adsorbed also showed an upward trend. Micropores, well-known for their benefit in CO_2 adsorption (Igalavithana et al. 2020), exhibited a positive linear relationship, as evident in the impressive R^2 = 0.9914 displayed in Fig. 5b. Notably, 2KC, with the largest mesopore distribution, stands out as the sample with the highest adsorbed CO_2 content, further emphasizing the crucial role of mesopores in CO_2 adsorption. One assumption could be that the effect of CO_2 diffusion in the mesopore is more important than the adsorption in micropores, thus rendering 2KC as the optimum sample for CO_2 adsorption. Based on this, preparing engineered biochar with specific pore size distributions may be an innovative research direction towards improving CO_2 adsorption.

Table 1
Langmuir and Freundlich model fitting parameters based on CO_2 adsorption isotherms at 298 K.

Samples	Langmuir			Freundlich		
	$q_e=(bq_0Ce)/(1+bC_e)$			$q_e=K_fC_e^{1/n}$		
	b	q_0	R^2	K_f	n	R^2
0KC	201.2484	145.4123	**0.99526**	940.6965	2.0141	0.99259
2KC	96.48074	290.3612	0.99562	2368.545	1.62237	**0.99918**
4KC	92.94251	267.1395	0.99534	2176.582	1.61222	**0.99938**
6KC	92.31406	258.0311	0.99521	2083.753	1.61548	**0.99947**
Isotherm modes parameters abbreviations used are listed in SI.						

3.3 Electrochemical performance

Figure 6 illustrates a distinct increase in electrochemical capacity of the A-xKC samples, characterized by rectangular CV shapes and triangular GCD shapes, both typical of Electric Double-Layer Capacitor (EDLC) electrode materials (Trinh et al. 2020). A-xKC had a capacitance of both CV and GCD greater than 160 F g^{-1}, which is considered better than biochar prepared from some bark materials such as willow bark (Hobisch et al. 2020), tree bark (Momodu et al. 2017). Previous studies showed that samples with large specific surface areas and micropores volumes, particularly those with sizes smaller than 1 nm, significantly contribute to enhancing the electrochemical capacity of the adsorbent when a sodium ion-based organic electrolyte is used (Thangavel et al. 2017). Additionally, hierarchical structures formed from micro-meso-macropores are reported to effectively increase the electrochemical capacity of adsorbent materials (Trinh and Tsubota, 2023). In this study, all A-xKC samples had micropore size distribution smaller than 1 nm as shown in MP plots and hierarchical structures formed from micro-meso-macropores as discussed in Fig. 3, so S_{BET} is believed to be the primary factor enhancing the electrochemical ability of A-xKC samples. Specifically, the 6KC sample, with the largest S_{BET}, micropore volume, and macropores (as analyzed in Fig. 2b and Fig. 3), achieved the most stable CV and GCD results under both fast scan rates of CV measurements and high current densities of GCD measurements. Small humps on CV shapes in Fig. 6a and longer discharge lines in GCD figures are attributed to the chemical reaction of basic functional groups (carbonyl and quinone) on the sample surface and protons (H^+) in the acidic aqueous solution, creating pseudo-capacitances (Oh et al. 2014). However, as discussed in Fig. 1, 2KC had the highest content of functional groups but also the lowest content of aromatic carbon structures, so it is possible that the content of basic functional groups, especially quinone groups, in 2KC is lower than 6KC, leading to the result that 2KC had an unstable GCD result compared to 6KC. Trinh et al. 2023 also reported that selective mesopore size (2–4 nm in diameter) would be more effective for supercapacitor application in the case of 1 M H_2SO_4 aq. electrolyte (Trinh and Tsubota 2023) and better van der Waals forces for physisorption as explained in Raman spectra, confirming the highest electrochemical performance of 6KC. Figure 7a presents the durability of the 6KC material through 50 CV curves at 1 mV s^{-1} and the corresponding capacitance retentions. The increased capacitance values observed after the first cycle are attributed to the heightened wettability of the electrochemical cells, aligning with findings from previous studies (Onodera and Tsubota 2022). Remarkably, after 50 cycles, the shape and size of the curves exhibited minimal changes, especially the size of the humps, providing compelling evidence for the stability of the material. Figure 7b displays the Ragone plots of 6KC in comparison to different energy storage devices (Liu et al. 2018; Wu et al. 2020), showcasing a maximum energy of *ca.* 11 Wh kg^{-1} and a maximum power of *ca.* 223 W kg^{-1} indicating that 6KC may be suitable for supercapacitor application. While not achieving excellence, this outcome lays the groundwork for future research endeavors aimed at enhancing the material's applicability.

4. Conclusion

In conclusion, the environmentally-friendly synthesis of porous biochar materials, derived from industrial waste Japanese cedar bark (JCB) and activated with the eco-friendly agent K_2CO_3, has proven to be

highly promising for applications in both CO_2 adsorption and supercapacitors. The study highlighted the role of the surface functional groups and pore structures in shaping the adsorption capacity of xKC. Particularly, 2KC exhibited exceptional chemisorption capacity, attributed to its rich functional groups and the largest pore volume (*ca.* 0.93 $cm^3\ g^{-1}$), resulting in an impressive CO_2 adsorption capacity of approximately *ca.* 180 mg g^{-1}. Furthermore, the electrochemical prowess of the materials was assessed, with 6KC showcasing superior stability under high scan rates and current densities. This performance was linked to its heightened physisorption ability, characterized by the largest ordered carbon structure content, maximum specific surface area (S_{BET}), and optimal pore sizes conducive to ion adsorption in a 1M H_2SO_4 electrolyte. The peak capacitance of 6KC reached an impressive *ca.* 210 F $g^{-}1$ at 10 mA g^{-1}. The study's findings offer valuable insights into the multifaceted capabilities of K_2CO_3-activated biochar sourced from JCB, illuminating the intricate relationship between material properties, CO_2 adsorption efficacy, and electrochemical behavior. This research not only expands our understanding of sustainable biomass-based materials but also lays the groundwork for diverse interdisciplinary applications, representing a noteworthy advancement in the sustainable and efficient utilization of biomass waste.

Declarations

Ethics approval

Not applicable. There are no involving human participants, their data or biological material in this research.

Consent to participate

Informed consent was obtained from all individual participants included in the study.

Consent to publish

The participant has consented to the submission of the case report to the journal.

Author Contributions

Conceptualization, Methodology: Toshiki Tsubota, Kieu Trang Trinh; Formal analysis and investigation, Writing - original draft preparation: Kieu Trang Trinh; Writing - review and editing: Kieu Trang Trinh, Dimitrios Kalderis, Toshiki Tsubota; Supervision: Toshiki Tsubota. All authors read and approved the final manuscript.

Funding

The authors declare that no funds, grants, or other support were received during the preparation of this manuscript.

Competing Interests

The authors have no relevant financial or non-financial interests to disclose.

References

1. Chen Z, Wang X, Xue B, et al (2020) Rice husk-based hierarchical porous carbon for high performance supercapacitors: The structure-performance relationship. Carbon 161:432–444. https://doi.org/10.1016/j.carbon.2020.01.088
2. Heidarinejad Z, Dehghani MH, Heidari M, et al (2020) Methods for preparation and activation of activated carbon: a review. Environ Chem Lett 18:393–415. https://doi.org/10.1007/s10311-019-00955-0
3. Hobisch MA, Phiri J, Dou J, et al (2020) Willow Bark for Sustainable Energy Storage Systems. Materials 13:1016. https://doi.org/10.3390/ma13041016
4. Igalavithana AD, Choi SW, Shang J, et al (2020) Carbon dioxide capture in biochar produced from pine sawdust and paper mill sludge: Effect of porous structure and surface chemistry. Science of The Total Environment 739:139845. https://doi.org/10.1016/j.scitotenv.2020.139845
5. Khoshraftar Z, Masoumi H, Ghaemi A (2023) Characterization and evaluation of low-cost biomass-based-AC for CO_2 capture: A review. Case Studies in Chemical and Environmental Engineering 8:100373. https://doi.org/10.1016/j.cscee.2023.100373
6. Khuong DA, Trinh KT, Nakaoka Y, et al (2022) The investigation of activated carbon by K_2CO_3 activation: Micropores- and macropores-dominated structure. Chemosphere 299:134365. https://doi.org/10.1016/j.chemosphere.2022.134365
7. Kim M-J, Choi SW, Kim H, et al (2020) Simple synthesis of spent coffee ground-based microporous carbons using K_2CO_3 as an activation agent and their application to CO_2 capture. Chemical Engineering Journal 397:125404. https://doi.org/10.1016/j.cej.2020.125404
8. Liu J, Wang J, Xu C, et al (2018) Advanced Energy Storage Devices: Basic Principles, Analytical Methods, and Rational Materials Design. Advanced Science 5:1700322. https://doi.org/10.1002/advs.201700322
9. Momodu D, Madito M, Barzegar F, et al (2017) Activated carbon derived from tree bark biomass with promising material properties for supercapacitors. J Solid State Electrochem 21:859–872. https://doi.org/10.1007/s10008-016-3432-z
10. Oh YJ, Yoo JJ, Kim YI, et al (2014) Oxygen functional groups and electrochemical capacitive behavior of incompletely reduced graphene oxides as a thin-film electrode of supercapacitor. Electrochimica Acta 116:118–128. https://doi.org/10.1016/j.electacta.2013.11.040
11. Onodera H, Tsubota T (2022) Dependence of pore structure of activated carbon on the performance of electrical double layer capacitor with NaCl aqueous electrolyte. J Porous Mater. https://doi.org/10.1007/s10934-022-01407-x
12. Teoh KS, Melchiorre M, Kreth FA, et al (2023) γ-Valerolactone as Sustainable and Low-Toxic Solvent for Electrical Double Layer Capacitors. ChemSusChem 16:e202201845.

https://doi.org/10.1002/cssc.202201845

13. Thangavel R, Kaliyappan K, Ramasamy HV, et al (2017) Engineering the Pores of Biomass-Derived Carbon: Insights for Achieving Ultrahigh Stability at High Power in High-Energy Supercapacitors. ChemSusChem 10:2805–2815. https://doi.org/10.1002/cssc.201700492
14. Trinh KT, Tsubota T (2023) Supercapacitors composed of Japanese cedar bark-based activated carbons with various activators. Materials Chemistry and Physics 307:128148. https://doi.org/10.1016/j.matchemphys.2023.128148
15. Trinh TK, Tsubota T, Takahashi S, et al (2020) Carbonization and H_3PO_4 activation of fern Dicranopteris linearis and electrochemical properties for electric double layer capacitor electrode. Sci Rep 10:19974. https://doi.org/10.1038/s41598-020-77099-7
16. Wu D, Xie X, Zhang Y, et al (2020) MnO_2/Carbon Composites for Supercapacitor: Synthesis and Electrochemical Performance. Frontiers in Materials 7:
17. Yang X, Igalavithana AD, Oh S-E, et al (2018) Characterization of bioenergy biochar and its utilization for metal/metalloid immobilization in contaminated soil. Science of The Total Environment 640–641:704–713. https://doi.org/10.1016/j.scitotenv.2018.05.298
18. Yue C, Tang Y, Qi W, et al (2023) Influences of Na_2CO_3, $NaHCO_3$, K_2CO_3 on the rheological, water distribution, and microstructural properties of 5% long-chain inulin dough and quality of steamed bread. LWT 176:114501. https://doi.org/10.1016/j.lwt.2023.114501
19. Yue L, Xia Q, Wang L, et al (2018) CO_2 adsorption at nitrogen-doped carbons prepared by K_2CO_3 activation of urea-modified coconut shell. Journal of Colloid and Interface Science 511:259–267. https://doi.org/10.1016/j.jcis.2017.09.040
20. Zhou X, Yue X, Tian C (2024) Responses of Ecosystem Productivity to Anthropogenic Ozone and Aerosols at the 2060. Earth's Future 12:e2023EF003781. https://doi.org/10.1029/2023EF003781

Figures

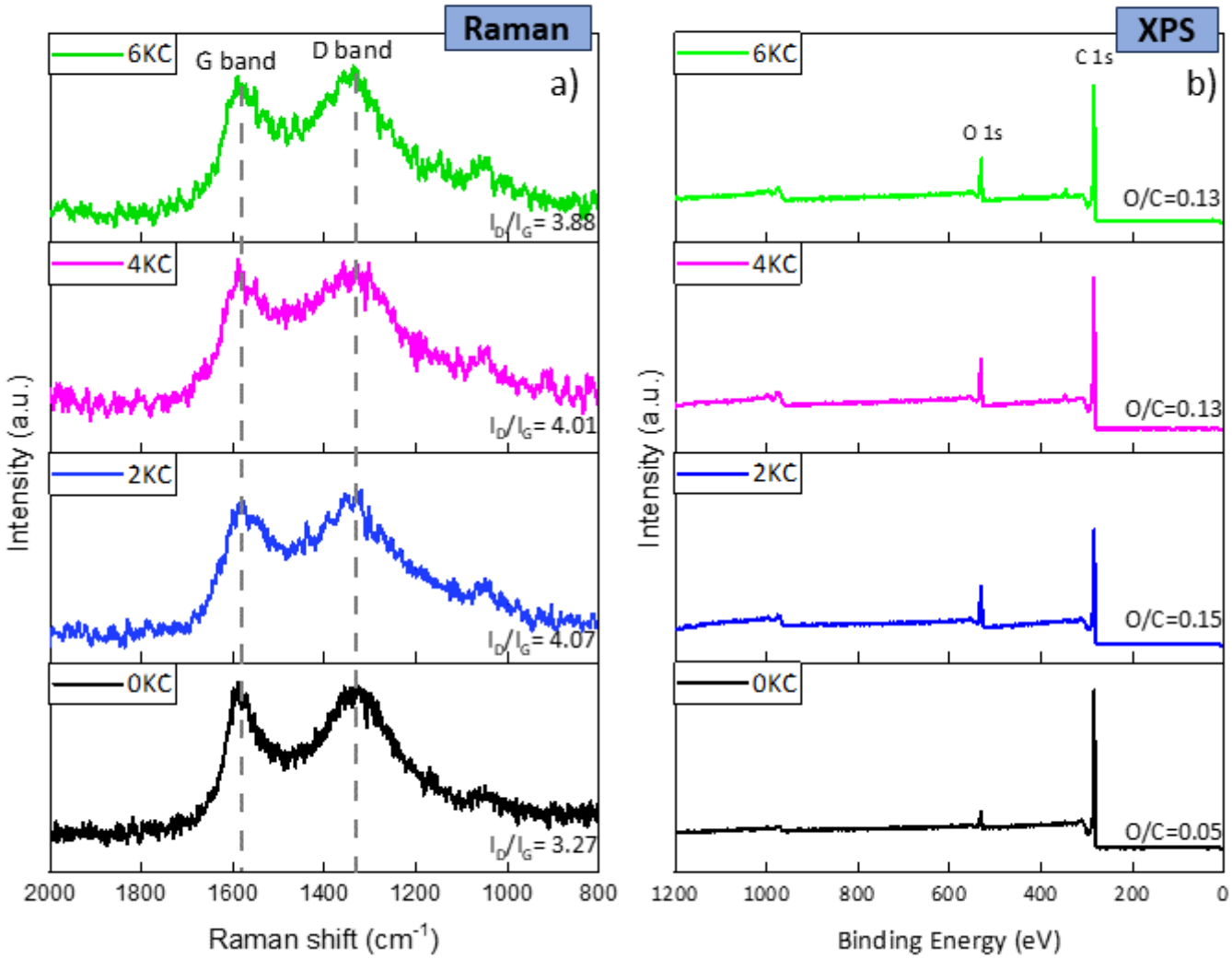

Figure 1

a) Raman and b) XPS spectra of K_2CO_3 -activated biochar

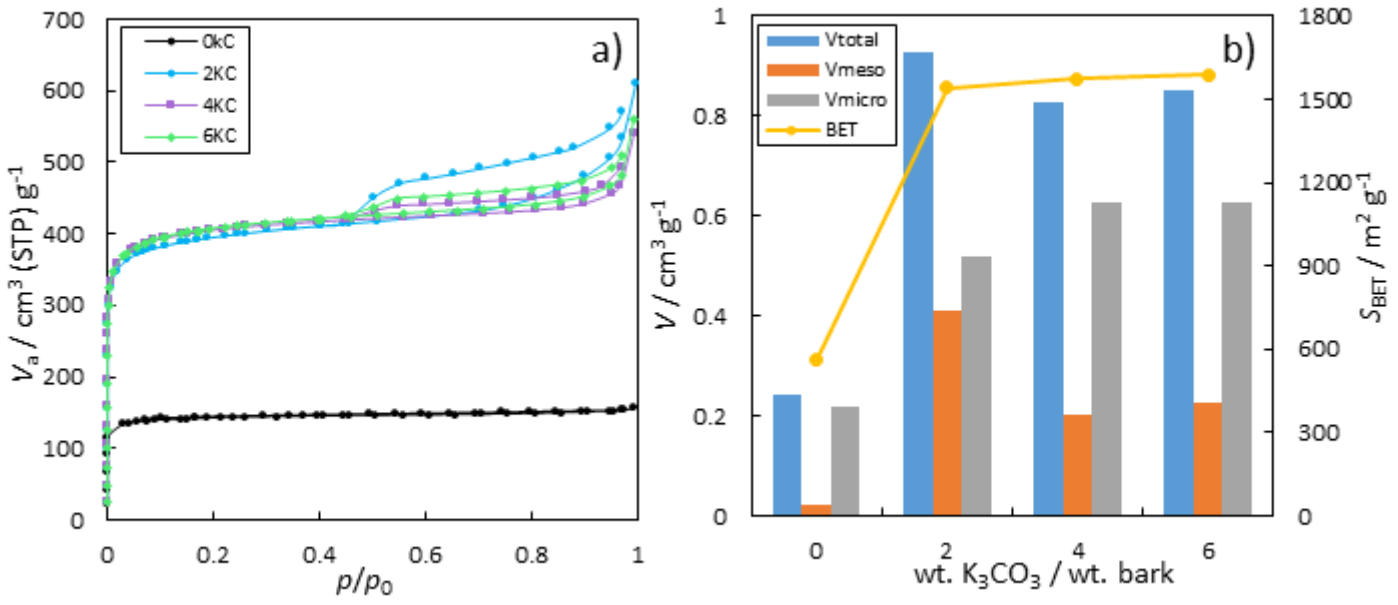

Figure 2

a) N_2 adsorption isotherms at 77 K, and b) BET specific surface area and pore volumes of K_2CO_3 - activated biochar

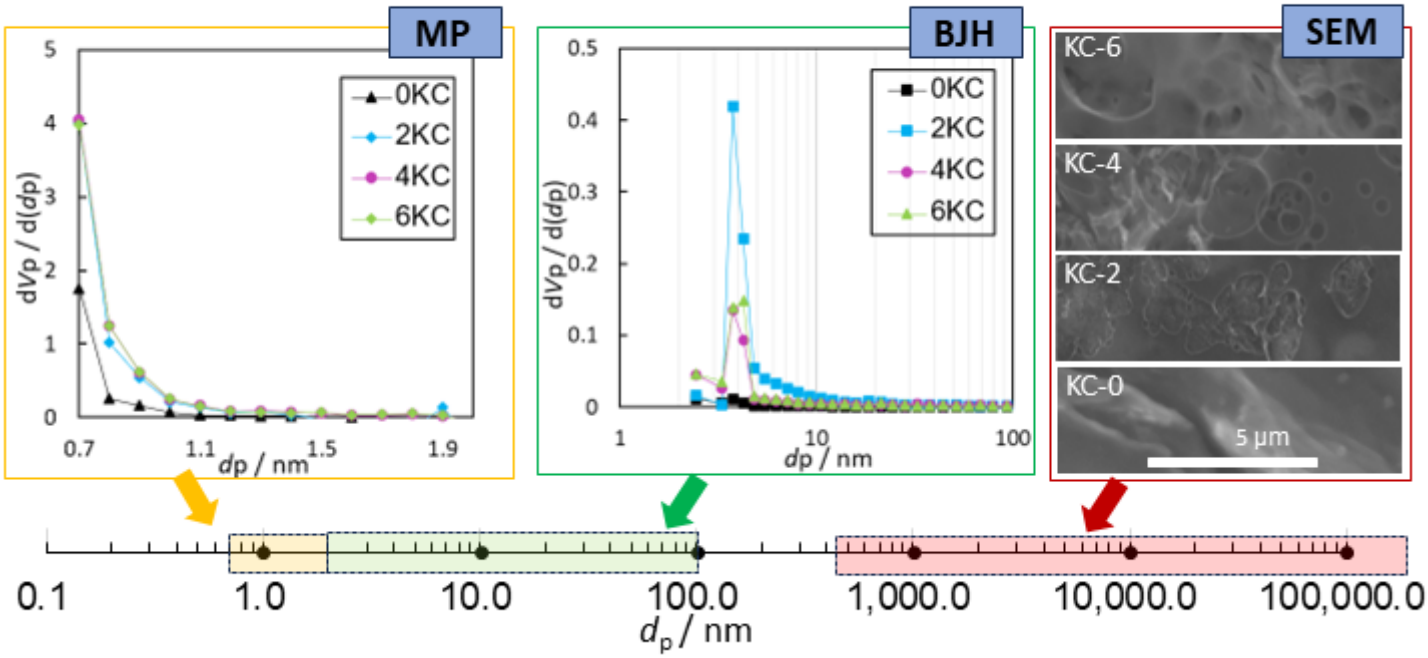

Figure 3

Pore-size distributions of K_2CO_3 -activated biochar demonstrated by MP, BJH plots and SEM images

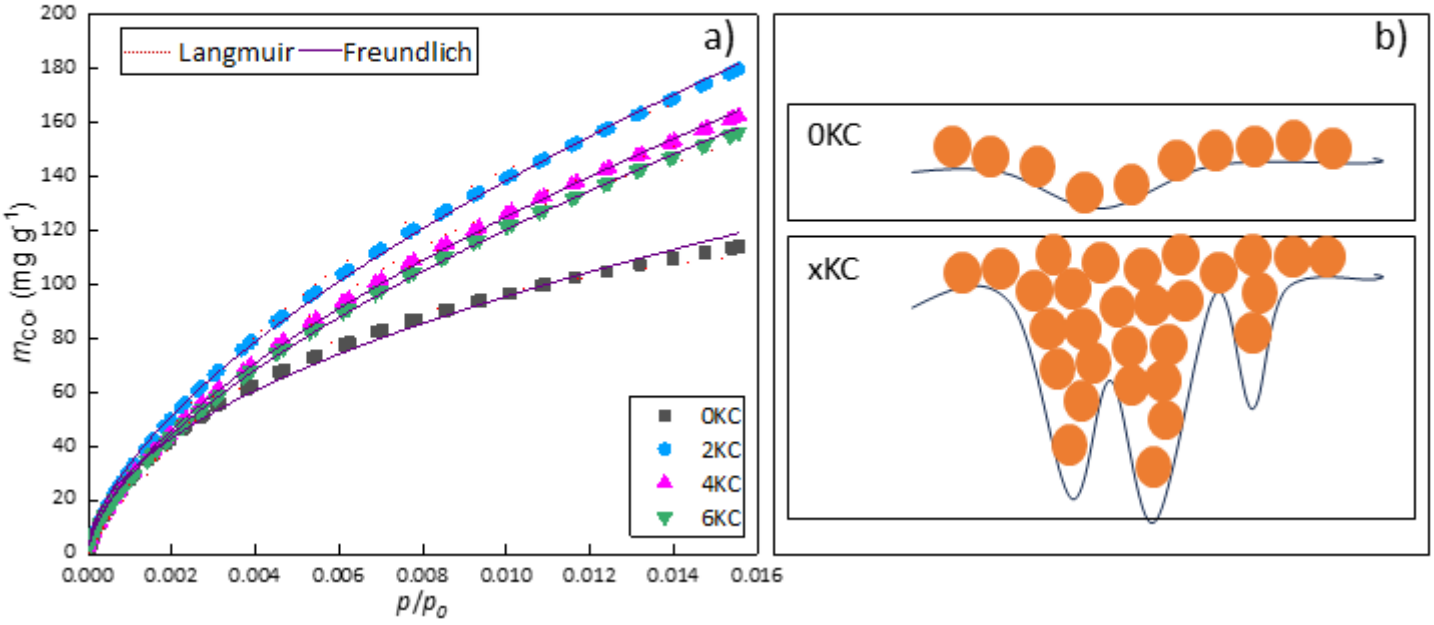

Figure 4

a) Langmuir and Freundlich model fittings based on CO_2 adsorption isotherms at 298 K, b) Diagram of CO_2 molecular in different pore structure of K_2CO_3 -activated biochar

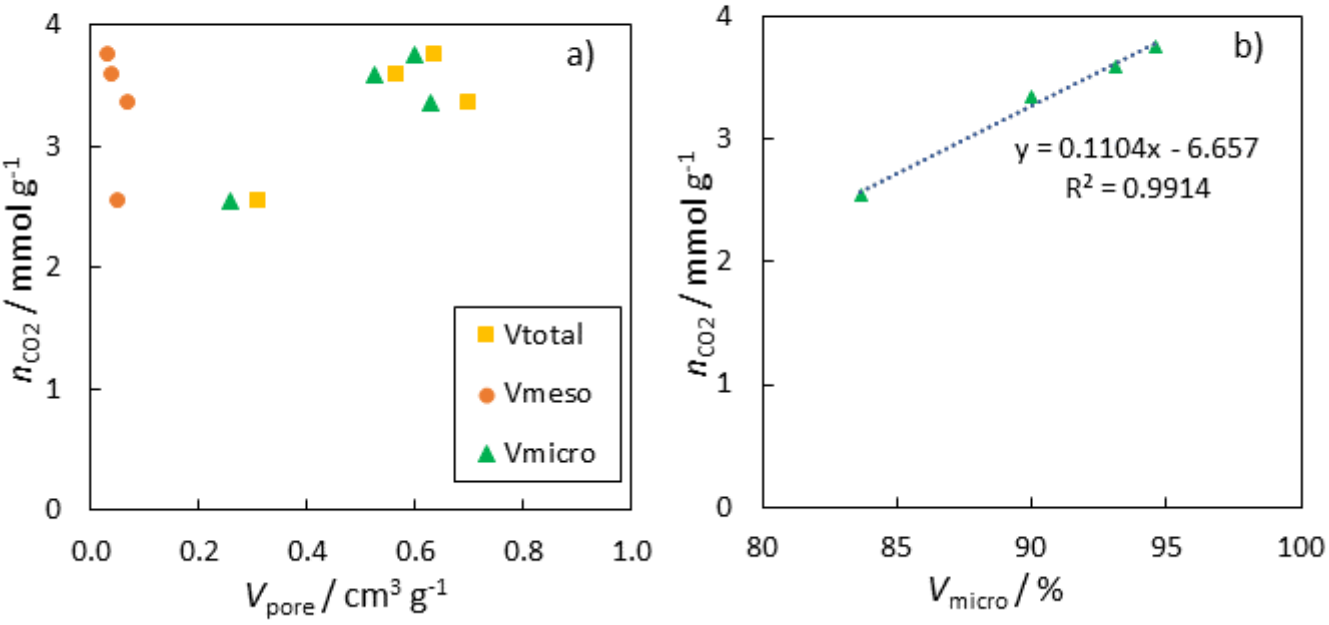

Figure 5

a) the relationship between pore volumes and CO_2 adsorption amount, and b) the correlation of the percentages of micropore volumes and CO_2 adsorption amount

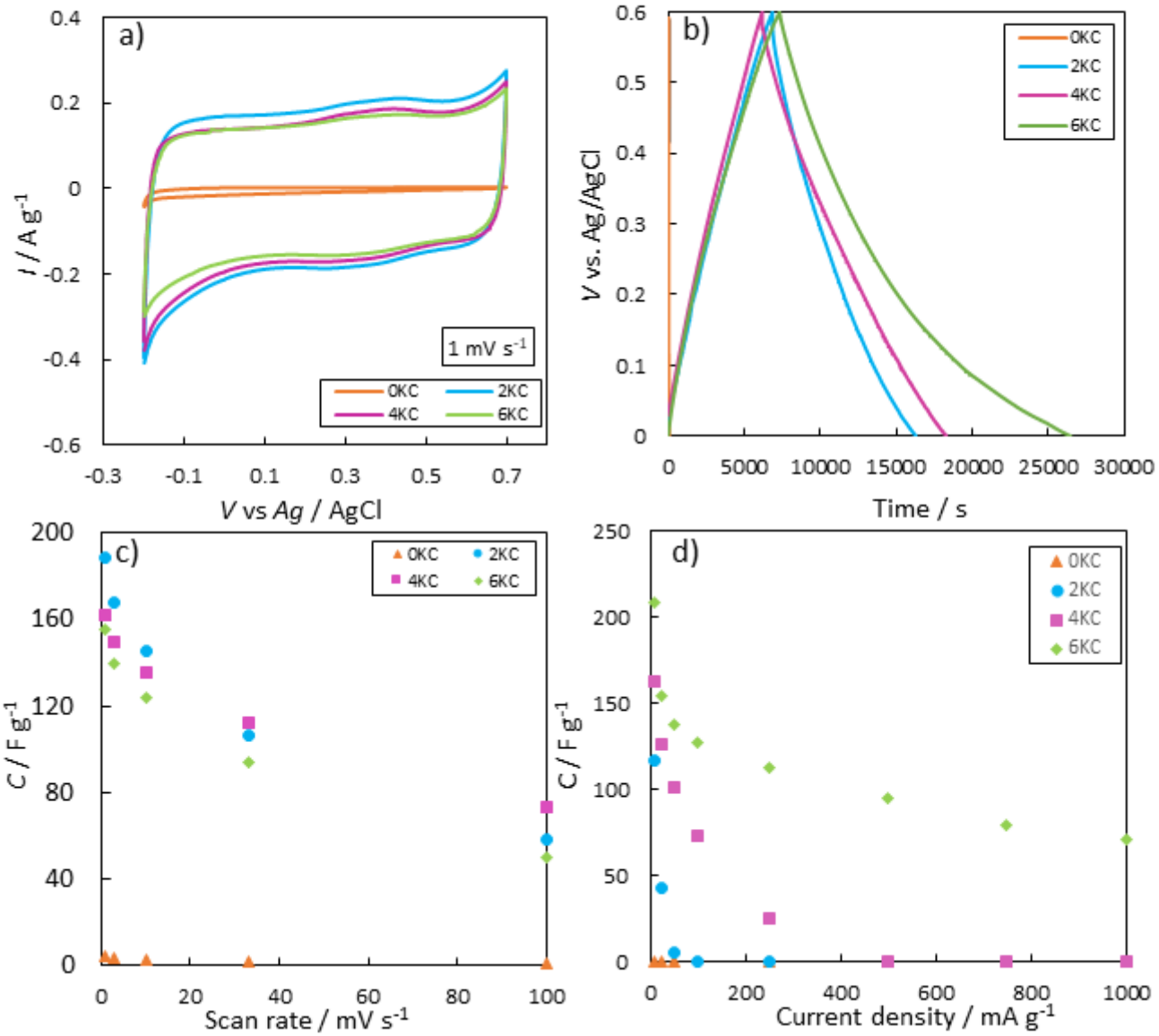

Figure 6

a) CV curves at the scan rate 1 mV s^{-1}, b) GCD curves at the current density 10 mA g^{-1}, c) capacitance calculated from CV data at different scan rates, and d) capacitance calculated from GCD data at different current densities

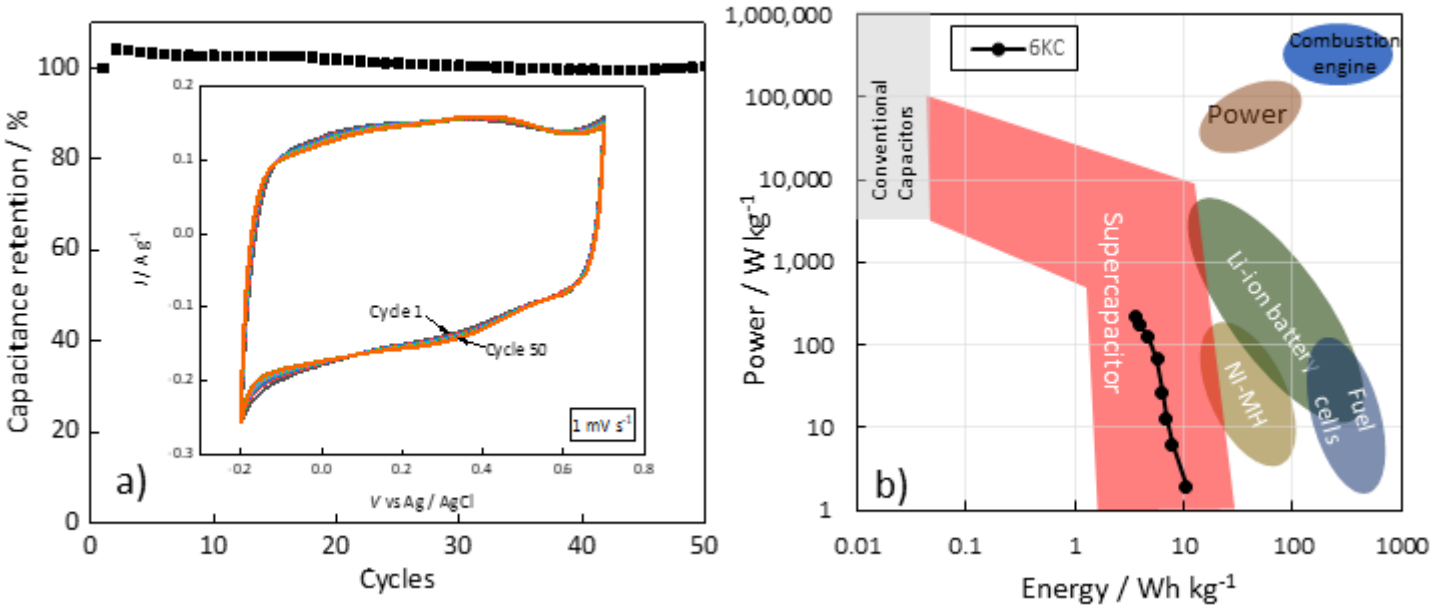

Figure 7

a) 50 CV cycles of 6KC at 1 mV s^{-1} and those capacitance retentions,

b) Ragone plot of 6KC comparing the power-energy characteristics and charge/discharge times of different energy storage devices

Supplementary Files

This is a list of supplementary files associated with this preprint. Click to download.

- Slide1.png
- 4.SupplementaryInformationESPRIEESspecialissue.docx